View metadata, citation and similar papers at core.ac.uk
brought to you by CORE
provided by Samara University

ANALYTICAL MODELING OF SYNCHRONOUS DEMODULATION OF A MULTI-DOF GYRO-ACCELEROMETER

Payal Verma [1], S.A. Fomchenkov [1], S.N. Khonina [1], N.L. Kazanskiy [1], R.V. Skidanov [1], R. Gopal [2]
[1] Samara State Aerospace University, Samara, Russia
[2] *CSIR – Central Electronics Engineering Research Institute, Pilani, India*

This paper reports a analytical model of a 4-DOF gyro-accelerometer consisting of 2-DOF drive and 2-DOF sense oscillators configured orthogonally. A detection scheme for time varying angular rate and linear acceleration, by combining the structural-model of gyro-accelerometer with the processes of synchronous demodulation and filtration, has also been spelt out to investigate frequency responses at the event of angular motion and linear acceleration. Finally, the results of the model have been validated by comparing with MATLAB®/Simulink data which shows excellent matching with each other.

Keywords: MEMS, Gyro-accelerometer, Synchronous demodulation.

Introduction

It is a well-known fact that all vibratory gyroscopes operate on the basis of transfer of energy from one mode to the other. The device may have either single DOF [1] or multi-DOF oscillators [2-4] which act as two orthogonally configured subsystems, a self-tuned oscillator forming the drive mode and a micro-g accelerometer, forming the sense mode. In the event of an angular rate, the transfer of energy from one mode to the other is detected and processed using suitable circuitry to produce the desired output. It is quite obvious that all vibratory gyroscopes can also sense linear acceleration in addition to angular rate sensing at their events of occurrence. Considering the strategy of simultaneous detection of linear acceleration and angular rate at their events, a controller circuit has been reported for a 2-DOF conventional gyroscope [5]. Some multi-DOF systems have also been proposed and realized which can sense linear acceleration along with angular rate [6, 7], while offering other advantages such as increased robustness and immunity to fabrication imperfections.

For the development of superior performance inertial sensors, the characteristics of the device have to be thoroughly understood and the design optimized which can achieved by taking proper care in the design and modeling stages. Hence mathematical modeling plays a key role in device design. Various mathematical models have been reported separately for accelerometer and gyroscope devices. Some of the mathematical models for gyroscopes have reported acceleration effect as an error, however confirming its presence. Recently, mathematical models of multi-DOF structures for simultaneous detection of acceleration effect and angular rate have also been reported, few of them are, 2-DOF gyro-accelerometer [8], a 2-DOF drive and 1-DOF sense gyro-accelerometer [6, 9, 10] and a 1-DOF drive and 2-DOF sense gyro-accelerometer [7].

4-DOF Model

The 4-DOF gyro-accelerometer system exploits the dynamic amplification in the decoupled 2-DOF drive and sense oscillators so as to attain large amplitude of oscillation without resonance [11]. Each of both 2-DOF drive and sense oscillators has two resonance peaks and flat zone in between peaks. The most important requirement of the overall 4-DOF gyro-accelerometer system is that the flat amplitude regions of both the 2-DOF oscillators must overlap precisely and the operating frequencies of the system must be located in their flat amplitude zones, thereby leading to the maximum robustness of the performance against the fluctuations of system parameters. The equations of motion can be represented by Newton's second law of motion, [2, 11]:

$$m_1\ddot{x}_1 + c_{1x}\dot{x}_1 + (k_{1x} + k_{2x})x_1 = k_{2x}x_2 + F_d(t)\,, \tag{1}$$

$$M_p\ddot{x}_2 + c_{2x}\dot{x}_2 + k_{2x}x_2 = k_{2x}x_1, \tag{2}$$

$$m_2\ddot{y}_2 + c_{2y}\dot{y}_2 + \left(k_{2y} + k_{3y}\right)y_2 = k_{3y}y_3 - 2m_2\Omega_z\dot{x}_2$$

$$-m_2\dot{\Omega}_z x_2 + m_2(a_x \sin\theta - a_y \cos\theta), \tag{3}$$

$$m_3\ddot{y}_3 + c_{3y}\dot{y}_3 + k_{3y}y_3 = k_{3y}y_2 - 2m_3\Omega_z\dot{x}_2$$

$$-m_3\dot{\Omega}_z x_2 + m_3(a_x \sin\theta - a_y \cos\theta), \tag{4}$$

Detection Scheme

The scheme for the discrimination of the angular rate and acceleration is presented below. This scheme for angular rate amplitude, Ω_o, and associated frequency, α, along with linear acceleration is applicable in case where angular rate is time dependent. The absolute transformation of (4) yields the solution that comprises both temporally damped and un-damped terms. The temporal decay terms, however, are not trivial as these are vital for deciding the turn-on time and settling time of the system. Since the output signal is processed after the device output is settled down, the contributions of decay terms become insignificant. Therefore the settled solution, of (4), is written as:

$$\bar{y}_3(t) = A_1 \cos\left\{(\omega + \alpha)t + \phi_{cx}(\omega) + \phi_{2y}(\omega + \alpha) + \phi_{cy}(\omega + \alpha)\right\}$$

$$+A_2 \cos\left\{(\omega - \alpha)t + \phi_{cx}(\omega) + \phi_{2y}(\omega - \alpha) + \phi_{cy}(\omega - \alpha)\right\}$$

$$+\mathcal{R}_{ex}\mathcal{A}_{2y}(\omega)\mathcal{A}_{cy}(\omega)\sin\left(\omega t + \phi_{2y}(\omega) + \phi_{cy}(\omega)\right), \tag{5}$$

where $\mathcal{R}_{ex}$, external acceleration and,

$$A_{1,2} = -\Omega_o f_o \omega_{2x}^2 \mathcal{A}_{cx}(\omega)\left(\omega \pm \frac{1}{2}\alpha\right)\mathcal{A}_{2y}(\omega \pm \alpha)\mathcal{A}_{cy}(\omega \pm \alpha),$$

$$\mathcal{A}_{cx}^{-2}(\omega) = [(\omega_{1x}^2 - \omega^2)(\omega_{2x}^2 - \omega^2) - \mu_x^2\omega_{2x}^4 - 4\lambda_{1x}\lambda_{2x}\omega^2]^2$$

$$+4[\lambda_{1x}(\omega_{2x}^2 - \omega^2)\omega + \lambda_{2x}(\omega_{1x}^2 - \omega^2)\omega]^2,$$

$$\phi_{cx}(\omega) = -\tan^{-1}\frac{2\omega\{\lambda_{1x}(\omega_{2x}^2 - \omega^2) + \lambda_{2x}(\omega_{1x}^2 - \omega^2)\}}{(\omega_{1x}^2 - \omega^2)(\omega_{2x}^2 - \omega^2) - \mu_x^2\omega_{2x}^4 - 4\lambda_{1x}\lambda_{2x}\omega^2},$$

$$\mathcal{A}_{cy}^{-2}(\omega)$$

$$+4\left[\lambda_{2y}\left(\omega_{3y}^2 - \omega^2\right)\omega + \lambda_{3y}\left(\omega_{2y}^2 - \omega^2\right)\omega\right]^2,$$

$$\phi_{cy}(\omega) = -\tan^{-1}\frac{2\omega\{\lambda_{2y}(\omega_{3y}^2-\omega^2)+\lambda_{3y}(\omega_{2y}^2-\omega^2)\}}{(\omega_{2y}^2-\omega^2)(\omega_{3y}^2-\omega^2)-\mu_y^2\omega_{3y}^4-4\lambda_{2y}\lambda_{3y}\omega^2},$$

$$\mathcal{A}_{2y}^2(\omega) = \left[\left(\omega_{2y}^2+\omega_{3y}^2-\omega^2\right)^2+4\lambda_{2y}^2\omega^2\right],$$

$$\phi_{2y}(\omega) = \tan^{-1}\frac{2\lambda_{2y}\omega}{\omega_{2y}^2+\omega_{3y}^2-\omega^2},$$

$$\omega_{1x}^2 = (k_{1x}+k_{2x})/m_1;\ \omega_{2x}^2 = k_{2x}/M_p,$$

$$\omega_{2y}^2 = (k_{2y}+k_{3y})/m_2;\ \omega_{3y}^2 = k_{3y}/m_3,$$

$$\mu_x^2\omega_{2x}^2 = k_{2x}/m_1;\ \mu_y^2\omega_{3y}^2 = k_{3y}/m_2; \mu_x^2 = M_p/m_1,$$

$$\mu_y^2 = m_3/m_2;\ f_o = F_o/m_1; \lambda_{1x} = c_{1x}/2m_1,$$

$$\lambda_{2x} = c_{2x}/2M_p;\ \lambda_{2y} = c_{2y}/2m_2;\ \lambda_{3y} = c_{3y}/2m_3.$$

As is evident from (5), the output signal is modulated by a sinusoidal function. The synchronous demodulation of this signal yields the in-phase and quadrature components defined as $\bar{y}_p = \bar{y}_3(t)\cos(\omega t)$ and $\bar{y}_q = \bar{y}_3(t)\sin(\omega t)$ respectively. In order to arrive at the low-pass-filtered solution after demodulation, we primarily deal with the in-phase component, $\bar{y}_p$. The quadrature component, $\bar{y}_q$, can be tackled accordingly. With the aid of trigonometric identities and settled solution (5), the in-phase component $\bar{y}_p$ is rearranged as,

$$\begin{aligned}\bar{y}_p &= \overline{A}\left\{\cos\left(2\omega t+\phi_{cx}(\omega)+\overline{\phi}\right)+\cos\left(\phi_{cx}(\omega)+\overline{\phi}\right)\right\}\cos(\alpha t+\Delta\phi)\\ &-\delta A\left\{\sin\left(2\omega t+\phi_{cx}(\omega)+\overline{\phi}\right)+\sin\left(\phi_{cx}(\omega)+\overline{\phi}\right)\right\}\sin(\alpha t+\Delta\phi)\\ &+\frac{1}{2}\mathcal{R}_{ex}\mathcal{A}_{2y}(\omega)\mathcal{A}_{cy}(\omega)\left\{\sin\left(\phi_{2y}(\omega)+\phi_{cy}(\omega)\right)\right.\\ &\qquad\left.+\sin\left(2\omega t+\phi_{2y}(\omega)+\phi_{cy}(\omega)\right)\right\}, \qquad (6)\end{aligned}$$

The modified parameters included in (6), as per [6, 7], are defined as,

$$\bar{A} = \frac{1}{2}(A_1+A_2);\ \ \delta A = \frac{1}{2}(A_1-A_2),$$

$$\bar{\phi} = \frac{1}{2}\left[\phi_{2y}(\omega+\alpha)+\phi_{2y}(\omega-\alpha)+\phi_{cy}(\omega+\alpha)+\phi_{cy}(\omega-\alpha)\right],$$

$$\Delta\phi = \frac{1}{2}\left[\phi_{2y}(\omega+\alpha)-\phi_{2y}(\omega-\alpha)+\phi_{cy}(\omega+\alpha)-\phi_{cy}(\omega-\alpha)\right].$$

Further, the output signals terms $\cos(\alpha t+\Delta\phi)$ and $\sin(\alpha t+\Delta\phi)$ in (6) led by phase shift, $\Delta\phi$, are related to the angular rate. The phase shift, $\Delta\phi$, in these function is distorted by frequency, α. Hence, it is essential to employ low-pass-filtering in order to eliminate the terms having doubled frequency. Thus, the filtered solution after trigonometric manipulation is given by,

$$\bar{y}_{lp} = A_p\cos\left(\alpha t+\psi_p\right)$$

$$+\frac{1}{2}\mathcal{R}_{ex}\mathcal{A}_{2y}(\omega)\mathcal{A}_{cy}(\omega)\sin\left(\phi_{2y}(\omega)+\phi_{cy}(\omega)\right), \qquad (7)$$

$$A_p^2 = \overline{A}^2\cos^2\left(\overline{\phi}+\phi_{cx}(\omega)\right)+\delta A^2\sin^2\left(\overline{\phi}+\phi_{cx}(\omega)\right),$$

$$\psi_p = \Delta\phi + \Delta\varphi_p,$$

$$\Delta\varphi_p = \tan^{-1}\left[\frac{\delta A}{\overline{A}}\tan\left(\overline{\phi}+\phi_{cx}(\omega)\right)\right].$$

Similarly, the low-pass-filtered quadrature component after demodulation is written as,

$$\bar{y}_{lq} = A_q\cos\left(\alpha t+\psi_q\right)$$

$$+\frac{1}{2}\mathcal{R}_{ex}\mathcal{A}_{2y}(\omega)\mathcal{A}_{cy}(\omega)\cos\left(\phi_{2y}(\omega)+\phi_{cy}(\omega)\right), \qquad (8)$$

where,

$$A_q^2 = \overline{A}^2\sin^2\left(\overline{\phi}+\phi_{cx}(\omega)\right)+\delta A^2\cos^2\left(\overline{\phi}+\phi_{cx}(\omega)\right),$$

$$\psi_q = \Delta\phi + \Delta\varphi_q,$$

$$\Delta\varphi_q = -\tan^{-1}\left[\frac{\delta A}{\overline{A}}\cot\left(\overline{\phi}+\phi_{cx}(\omega)\right)\right].$$

Table 1. Parameter values used for calculations.

Parameters	**Values**
Active mass (m_1)	201.9 x 10^{-9} kg
Passive mass (m_2)	57.24 x 10^{-9} kg
Sense mass (m_3)	5.6 x 10^{-9} kg
Frame mass (m_f)	10.5 x 10^{-9} kg
Spring constant (k_{1x}; k_{2x})	153.5 N/m; 87.59 N/m
Spring constant (k_{2y}; k_{3y})	62.26 N/m; 6.1 N/m
Frequencies ($\omega_{1x} = \omega_{2x} =$	5.5 kHz
ω_{2y})	5.25 kHz
Frequency (ω_{3y})	2.171x10^{-5} N; 200 rad
F_o; Angular rate (Ω_o)	

Results

Considering the design equations, the spring constants and structural frequencies by adjusting mass values, m_1, m_2, m_3, frame mass, m_f and subsequently mass ratios, μ_x^2 and μ_y^2, have been decided optimally. The values of these and other parameters are listed in Table 1. The following figures have been calculated by using these values unless it is specified.

Figure 1a,b are Bode plots of the demodulated and low-pass-filtered in-phase and quadrature components of amplitudes of Coriolis and Euler's signal of gyro-accelerometer for different values of driving frequency.

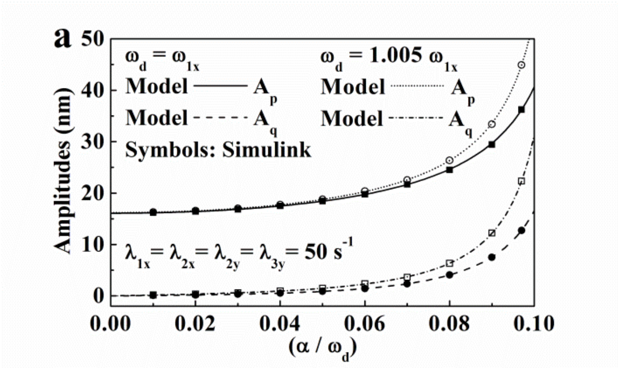

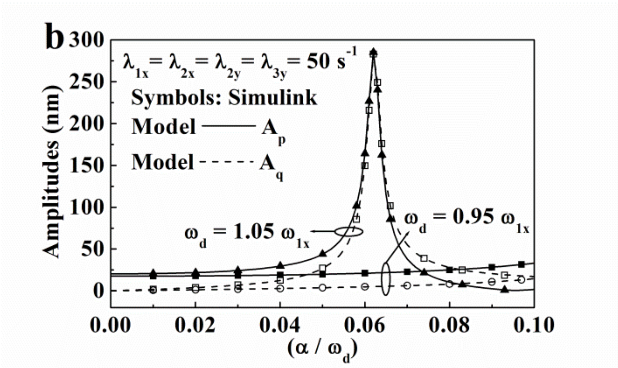

Fig. 1. Bode plots of demodulated and then filtered in-phase and quadrature components of amplitudes and corresponding phases, **a** amplitudes for $\omega = \omega_d = \omega_{1x}$ and for $\omega_d = 1.005\ \omega_{1x}$, **b** amplitudes for $\omega_d = 1.05\ \omega_{1x}$ and for $\omega_d = 0.95\ \omega_{1x}$, (symbols are Simulink results)

Conclusion

The simultaneous detection scheme of time varying angular rate and linear acceleration utilizes the synchronous demodulation that yields in-phase and quadrature output signals of the systems. In case of matched zero phase frequencies of both the oscillators, the associated acceleration term in in-phase component becomes ineffective and the device deliver only angular rate related signals, whereas the quadrature signal is dominant by acceleration action and that related to angular rate becomes almost insignificant. Therefore, in-phase signal can be used for acceleration detection and quadrature one for angular rate extractions. MATLAB®/Simulink model of the gyro-accelerometer system was developed in order to investigate the feasibility of such a detection scheme and simulation results have shown excellent correspondence with analytical results.

Acknowledgements

The work was partially funded by the Russian Federation Ministry of Education and Science, Russian Science Foundation, Presidential grants for support of leading scientific schools and Russian Foundation of Basic Research Grants.

References

1. Alper SE, Akin T. Symmetrical and decoupled nickel microgyroscope on insulating substrate. Sensors and Actuators A: Physical 2004; 115: 336-350.

2. Acar C, Shkel A. MEMS vibratory gyroscopes-structural approaches to improve robustness, Springer, Berlin, 2009.
3. Verma P, Gopal R, Butt MA, Khonina SV, Skidanov RV. Design and simulation of non-resonant 1-DOF drive mode and anchored 2-DOF sense mode gyroscope for implementation using UV-LIGA process. In: Proceedings of the SPIE 9807, 2016; doi:10.1117/12.2231372.
4. Verma P, Juneja S, Savelyev DA, Khonina SN, Gopal R. Design and fabrication of a 1-DOF drive mode and 2-DOF sense mode micro-gyroscope using SU-8 based UV-LIGA process. In: Proceedings of the AIP 1724, 2016; doi: 10.1063/1.4945137.
5. Sung WT, Kang T, Lee JG. Controller design of a MEMS gyro-accelerometer with a single proof mass. International Journal of Control, Automation, and Systems 2008; 6(6): 873-883.
6. Verma P, Gopal R, Arya SK. Analytical modeling and simulation of a 2-DOF drive and 1-DOF sense gyro-accelerometer. Microsystem Technologies 2013; 19(8): 1238-1249.
7. Verma P, Arya SK, Gopal R. Lumped parameter analytic modeling and behavioral simulation of a 3-DOF MEMS gyro-accelerometer. Acta Mechanica Sinica 2015; 31(6): 910-919.
8. Verma P, Gopal R, Arya SK. Dynamic characteristics of vibratory gyro-accelerometer. In Proceeding of the IEEE, 5th International Conference on Computers and Devices for Communication, University of Calcutta, India, 2012; doi:10.1109/CODEC.2012.6509277.
9. Verma P, Agrawal P, Gopal R, Arya SK. Parametric sensitivity analysis of a 2-DOF drive and 1-DOF sense modes MEMS gyro-accelerometer structure. Advance Science Letters 2014; 20: 1495-1498.
10. Verma P, Khan KZ, Butt MA, Khonina SN, Kazanskiy NL, Gopal R. Acceleration Characterization of Dual Purpose Gyro/Accelerometer Device using MS3110 Differential Capacitive Read Out IC. *In* Proceeding *of IEEE*, MicroCom 2016, NIT Durgapur, India.
11. Verma P, Khan KZ, Gopal R, Butt MA, Fomchenkov SA, Savelyev DA, Khonina SN, Kazanskiy NL, Skidanov RV. Analytical modeling of a non-resonant muti-DOF MEMS gyro-accelerometer. *In* Proceeding *of the IEEE, ICECS 2016, Coimbatore, India.*